THE APPLICATION OF SANDSTONE TO REDUCE LIMESTONE ARMORING IN ACID MINE DRAINAGE

A Thesis by

Amy Teresa Bailey

Bachelor of Science, University of Oklahoma, 2016

Submitted to the Department of Earth, Environmental, and Physical Sciences
and the faculty of the Graduate School of
Wichita State University
in partial fulfillment of
the requirements for the degree of
Master of Science

May 2018

THE APPLICATION OF SANDSTONE TO REDUCE LIMESTONE ARMORING IN ACID MINE DRAINAGE

The following faculty members have examined the final copy of this thesis for form and content, and recommend that it be accepted in partial fulfillment of the requirement for the degree of Master of Science, with a major in Geology.

_____

Andrew Swindle, Committee Chair

_____

William Bischoff, Committee Member

_____

Mark Schneegurt, Committee Member

ACKNOWLEDGMENTS

First and foremost, I want to thank my advisor, Dr. Andrew Swindle, for his guidance and continuous support. Thank you for always encouraging me and making me a better scientist. Next, I want to thank Dr. William Bischoff and Dr. Mark Schneegurt for their insight and being part of my committee. Last but not least, I would like to thank all of those who have been by my side during this journey for always supporting me and for always being there.

ABSTRACT

Acid mine drainage (AMD) is a significant environmental problem in most countries that have an extensive history of mining. AMD refers to the acidic water that can be produced during hard and soft rock mining. Acidic drainage forms when sulfide minerals, primarily pyrite, are exposed to oxygenated surface waters. Passive limestone trenches are a common technique used to neutralize AMD through the dissolution of limestone and release of carbonate. The addition of carbonate to AMD causes the pH to rise due to the consumption of H^+ and results in precipitation of iron from AMD. In limestone trenches, the iron precipitate can adhere to limestone surfaces, armoring them, and limiting their ability to continue to neutralize AMD. In turn, this armoring lowers the effectiveness of the passive trench as an AMD remediation tool.

The goal of this research was to investigate if the presence of sandstone reduces the armoring of limestone during the AMD neutralization reaction, and, if armoring of the limestone is reduced, does the mineralogy of the sandstone play a role in this reaction. AMD neutralization batch reactions were run in which AMD was reacted with just limestone, limestone and iron oxide-cemented sandstone, and limestone and quartz-cemented sandstone. In the limestone only experiments, the AMD neutralized after ~4 days. However, in the experiments with limestone and sandstone, the AMD was neutralized in slightly less time. Additionally, light microscopy revealed that the presence of sandstone reduced the armoring of limestone grains. The experimental data suggests that the addition of sandstone did increase the rate of neutralization due to the iron precipitates adhering to the sandstone rather than the limestone. Also, quartz-cemented sandstone had a greater impact on neutralization reaction than did iron oxide-cemented sandstone.

TABLE OF CONTENTS

LIST OF TABLES

LIST OF FIGURES

I. INTRODUCTION

In the United States of America, commercial coal mining started in the 1740s, followed by commercial ore mining in the 1800s (Department of Energy; Department of Interior). The mining industry has been a large contributor to the US economy creating jobs, raw materials, and fossil fuels. However, mining activities also have several drawbacks. In particular, the prominent legacy problem of acid waters associated with mines and mine tailings known as acid mine drainage (AMD). AMD is an environmental hazard that can greatly impair the behavioral, reproduction, and ecological aspects of wildlife in a river system (Gray, 1997).

AMD characteristically has elevated concentrations of dissolved sulfate, iron, and other various metals, has an acidic pH, and can become toxic to humans and ecosystems (Akcil and Koldas, 2006; Robb and Robinson, 1995). AMD occurs in mine tailings, mine pits, and waste rock piles and is produced when sulfide minerals (e.g. pyrite, galena, sphalerite) are exposed to oxygenated waters (Iakovleva et al., 2015; Sasowsky et al., 2000). The Bureau of Land Management has confirmed over 52,200 abandoned mines and 97,600 specific features (Department of Interior) that have the potential to generate AMD and contaminate streams. Figure 1 shows a representative stream that has been impacted by AMD. The stream has the orange-yellow-red color that is characteristic of AMD due to the high concentration of dissolved and colloidal iron.

AMD, typically, has a pH between 2 and 6 and high acidity, which is reflective of the hydrogen ion concentration as well as the concentration of acid metal cations (i.e. Fe^{2+}, Fe^{3+}, Al^{3+}, Mn^{2+}). There are many factors that make AMD highly variable from site-to-site including the type of material being mined, trace mineral associations, and the lithology of the host rock. However, there are certain elements that can be found in most AMD such as iron, sulfate, and

aluminum (Burke and Banwart, 2002; Kairies et al., 2005; Nordstrom et al., 2017). Even coal mines generally have elevated concentrations of iron, sulfate, aluminum, and manganese in the wastewater (Robb and Robinson, 1995). The composition of the AMD, the concentration of each metal, the pH value, and the acidity are important factors when determining which treatment option will be the most effective in removing the metals and neutralizing the pH (Hedin et al., 1994; Skousen and Foreman, 1999). It is crucial to remove metals (especially iron) from the wastewater because acid metal cation hydrolysis, precipitation, and dissolution reactions act as strong pH buffer.

Figure 1: Stream in western Pennsylvania impacted by AMD. (Warner)

1.1 Iron Oxides

In this paper, the term 'iron oxide' is used to refer to any iron mineral containing O or OH as the main anionic. Iron oxides are common in the subsurface and can be produced in a number of ways such as the weathering of iron containing primary silicate minerals or by precipitation of iron from soil solutions (Brady and Weil, 2008). Common iron oxides include hematite (Fe_2O_3), magnetite (Fe_3O_4), and goethite (FeOOH). Iron oxides are often colloidal (1μm to 1nm) and composed of iron atoms coordinated with oxygen atoms and/or hydroxyl molecules in octahedral sheets (Cornell, 2006). The hydroxyl groups are chemically reactive at the surface of solids due to the double pair of electrons and a dissociable hydrogen; this allows for the hydroxyl groups to release or accept cations from the surrounding solution and result in an overall negative or positive charge on the surface of the solid.

1.2 AMD Chemistry

The composition of AMD will vary from mine to mine due differences in types of metals, available, their speciation and concentration, as well as site-specific environmental conditions such as pH and Eh. Most AMD has a high concentration of iron due to the common occurrence of iron sulfide minerals, such as pyrite (Akcil and Koldas, 2006). Pyrite is typically associated with coal because it is formed in reducing environments with a continuous supply of sulfates and iron in the presence of easily decomposable organic matter, and it is also associated with ore mines such as copper, gold, and silver because it is a common product of hydrothermal deposits. The molecular structure of pyrite can be described as having three parts: Fe(II), S_A, and S_B (Evangelou, 1995). The S_B section is exposed to the surface and contains an unshared pair of electrons, which produces a slight negative charge on the pyrite's surface. The negative charge

attracts molecules and cations to share/use the unshared electron. (Berner, 1970; Evangelou, 1995; Pyzik and Sommer, 1981; Wilkin and Barnes, 1996)

The oxidation of pyrite is the driving force for the formation of AMD.

$$FeS_2 + \frac{7}{2}O_2 + H_2O \rightarrow Fe^{2+} + 2H^+ + 2SO_4^{2-} \quad (1)$$

$$Fe^{2+} + \frac{1}{4}O_2 + H^+ \rightarrow Fe^{3+} + \frac{1}{2}H_2O \quad (2)$$

$$Fe^{3+} + 3H_2O \rightarrow Fe(OH)_{3(solid)} + 3H^+ \quad (3)$$

$$FeS_2 + 14Fe^{3+} + 8H_2O \rightarrow 15Fe^{2+} + 2SO_4^{2-} + 16H^+ \quad (4)$$

When pyrite (FeS_2) interacts with oxygen (O_2) and water (H_2O), the sulfur in the pyrite is oxidized, and the water is hydrolyzed resulting in the release of ferrous iron (Fe^{2+}), hydronium (H^+), and sulfate (SO_4^{2-}) ions into the water (Evangelou, 1995). This chemical reaction (1) results in the lowering of the water's pH due to the release of H^+ ions. In oxygenated waters, Fe^{2+} will be oxidized to ferric iron (Fe^{3+}) (Iakovleva et al., 2015). The iron-oxidizing bacteria (*Thiobacillus ferroxidans*) that are often present in AMD sites (Baker and Banfield, 2003; Barnes and Romberger, 1968; Benner et al., 2000) increase the rate of Fe^{2+} oxidation. This reaction (2) results in the use of an H^+ ion and the production of a water molecule (Evangelou, 1995). If the pH is greater than 4-4.5, Fe^{3+} will hydrolyze and precipitate into an iron (III) hydroxide ($Fe(OH)_3$) resulting in a reduction in pH due to the production of H^+ ions (3) (Iakovleva et al., 2015). However, Fe^{3+} ions can also catalyze the oxidation of additional pyrite resulting in additional Fe^{2+} and SO_4^{2-} ions in the water and lowering the pH by increasing the amount of H^+ ions in the water (4).

Acidity can be defined as a measurement of the base neutralization capacity of a solution. In addition to H^+, acid metal cations such as Fe^{2+}, Fe^{3+}, Al^{3+}, and Mn^{2+} add to the acidity of

AMD due to their ability to facilitate hydrolysis reactions that produce H^+ (8,9,10,11) (Watzlaf et al., 2004).

$$Fe^{2+} + \frac{1}{4}O_2 + \frac{3}{2}H_2O \rightarrow FeOOH + 2H^+ \quad (8)$$

$$Fe^{3+} + 2H_2O \rightarrow FeOOH + 3H^+ \quad (9)$$

$$Al^{3+} + 3H_2O \rightarrow Al(OH)_3 + 3H^+ \quad (10)$$

$$Mn^{2+} + \frac{1}{4}O_2 \rightarrow MnOOH + 2H^+ \quad (11)$$

These reactions can be used to calculate the total acidity of the AMD. The acidity is calculated from the pH of the AMD and the sum of the milliequivalents of the dissolved acidic metals (12) (Watzlaf et al., 2004).

$$Acid_{calc} = 50\left(\frac{2Fe^{2+}}{56} + \frac{3Fe^{3+}}{56} + \frac{3Al^{3+}}{27} + \frac{2Mn^{2+}}{55} + 1000(10^{-pH})\right) \quad (12)$$

In equation 12, all the metal concentrations are in mg/L, and 50 is the equivalent weight of $CaCO_3$, thus allowing for the conversion from mg/L of acidity into mg/L as $CaCO_3$ equivalent. After simplifying equation 12, the following equation (13) (Watzlaf et al., 2004) is obtained:

$$Acid_{calc} = 1.79[Fe^{2+}] + 2.68[Fe^{3+}] + 5.56[Al^{3+}] + 1.82[Mn^{2+}] + 50{,}000[10^{-pH}] \quad (13)$$

1.3 Passive AMD Neutralization in Limestone Trenches

Over the last 20 years, several different passive treatment systems have been developed such as constructed wetlands (McCauley et al., 2009), anoxic limestone trenches (Hedin et al., 1994), aerobic limestone trenches, bioreactors (García et al., 2001; Gibert et al., 2004) and permeable reactive barriers (Kaksonen and Puhakka, 2007; Neculita et al., 2007). The cost to implement these treatments processes can vary considerably depending on the engineering design and location, the chemistry and composition of the wastewater stream, and the discharge criteria. Limestone trenches are frequently used because of the lower costs in construction compared to the other treatments (Johnson and Hallberg, 2005). Anoxic limestone trenches are

built under ground while aerobic trenches are above ground. Since the aerobic trench is above ground, it costs less than implementing an anoxic trench (Cravotta Iii and Trahan, 1999; Gazea et al., 1995; Hedin et al., 1994).

In both the anoxic and open trenches, the limestone neutralizes AMD through dissolution and the release of carbonate (CO_3^{-2}) into solution.

$$CaCO_3(s) + H_2O \leftrightarrow Ca^{2+} + H^+ + CO_3^{2-} + OH^- \quad (5)$$

$$CO_3^{2-} + H^+ \leftrightarrow HCO_3^- \quad (6)$$

$$H_2CO_3 + H_2O \leftrightarrow HCO_3^- + H^+ \quad (7)$$

In acidic solutions, limestone will dissolve and release Ca^{2+} and CO_3^{2-} ions, and the water will hydrolyze producing H^+ and OH^- ions (5). Then, the H^+ will bind to the CO_3^{-2} to form HCO_3^- (6). With the increase in CO_3^{2-}, the chemical reaction (6) will shift to the right, consuming more H^+ and producing HCO_3^-. Figure 2 displays the dominant carbonate species in water as a function of pH. In a pH range of 6-10, HCO_3^- is the dominant species. Overall, the addition of calcium carbonate to AMD causes the pH to rise due to the consumption of H^+ to form bicarbonate. However, the increase in pH causes metal ions to precipitate out of solution causing armoring to occur on the remaining, undissolved limestone.

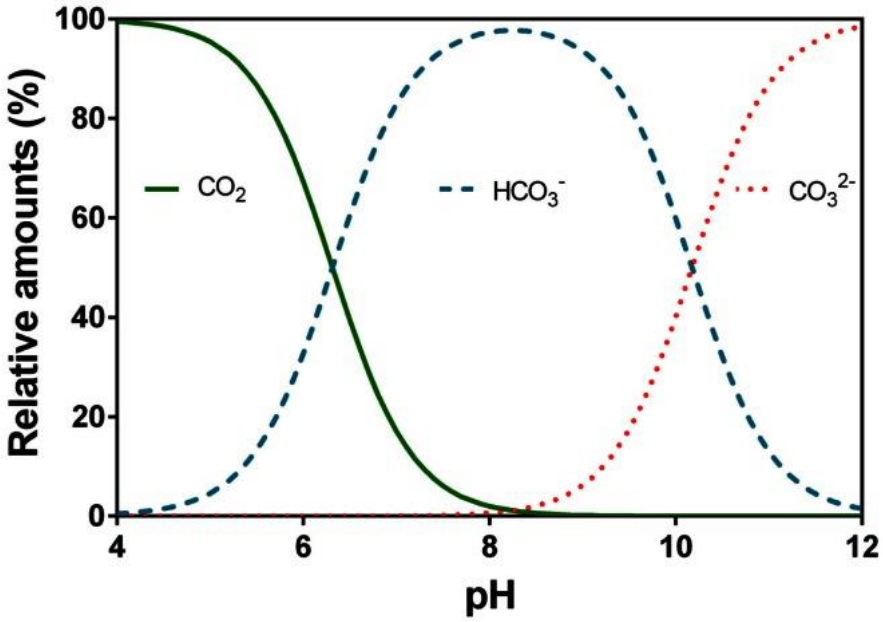

Figure 2: Dominate carbonate species in water as a function of pH (Ole et al., 2013)

1.3 Iron Solubility and Armoring

The speciation of iron in AMD is largely determined by the pH level and Eh of the drainage. Figure 3 is a Eh-pH field stability diagram for iron in equilibrium with diatomic oxygen at 1 atmosphere pressure (Lower, 2017). Under reducing conditions, Fe^{2+} is the dominant oxidation state, while under oxidizing conditions, Fe^{3+} tends to dominate. Ferric iron also has a lower solubility than ferrous iron and is only stable in aqueous form within a narrow range of Eh-pH conditions as shown in Figure 3. In addition, Figure 3 shows that under oxic conditions, as pH increases, the solubility of iron decreases. Thus, the neutralization of AMD by limestone, which raises pH, drives the Eh-pH conditions, so that dissolved iron is no longer stable. At pHs greater than ~4-4.5, Fe^{3+} will precipitate out as $Fe(OH)_3$, lowering the acidity of the AMD. Iron precipitation in AMD has been studied in depth, and several studies (Cravotta Iii and Trahan, 1999; Rose and Elliott, 2000; Sullivan, 1988) have demonstrated that the accumulation of solid precipitate can armor (i.e. cover) the limestone causing the neutralization of the AMD to decrease or stop.

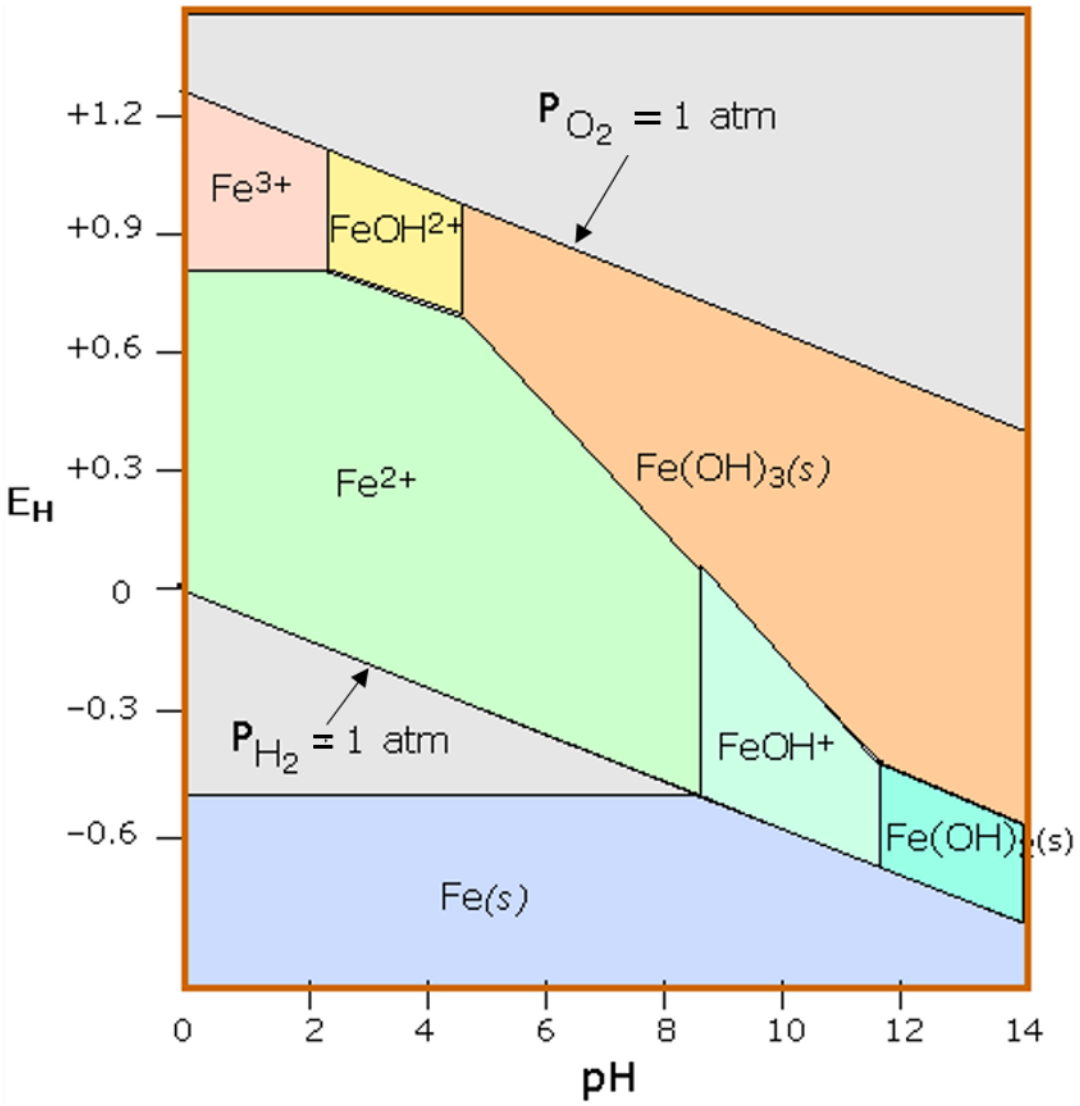

Figure 3: Stability-field diagram for aqueous ferric-ferrous system under 25°C and 1atm with no other ions in the solution. Modified from (Lower, 2017)

1.4 Objective

Previous studies (Sasowsky et al., 2000; Xu et al., 1997) have investigated using sandstone rather than limestone, or a mixture of sandstone and limestone in the neutralization of AMD to in an attempt to ameliorate the issue of the precipitation of iron oxides. In Sasowsky et al. (2000), the authors' reported that when using a combination of limestone and sandstone to neutralize AMD, the quartz-rich sandstone samples were more heavily coated with metal precipitates than the limestone samples. Additionally, it was reported that experiments

containing both sandstone and limestone resulted in a greater reduction in the amount of iron in the AMD than did experiments with limestone alone. However, the authors did not investigate if the mineralogy of the sandstones had an impact on the neutralization process. My research builds on this earlier work by investigating if the presence of sandstone effects the armoring of limestone during the AMD neutralization reaction, and if the mineralogy of the sandstone plays a role in this reaction.

II. ANALYTICAL METHODS

2.1 AMD Preparation

Synthetic Acid Mine Drainage (AMD) was prepared in the laboratory by dissolving ~350 mg of iron(III) sulfate hydrate in sufficient distilled deionized water to create 1-L of solution. The pH of the starting AMD solution varied from 2.18 to 2.72 between the four batches of solution.

2.2 Limestone and Sandstone Preparation

A benefit to passive limestone trenches is the relatively low-cost required to build and maintain the trenches. As such, this study used limestones and sandstones that were either locally available at or could be purchased for low cost. The limestone used in this research was commercially available from a local hardware supply store. While sandstone can contain a wide variety of cements, such as chlorite and pyrite (Berger et al., 2009; Burley and Worden, 2003), this research used iron oxide-cemented and quartz-cemented sandstones for the reasons described above. Our representative iron oxide-cemented sandstone was collected from an outcrop of the Garber Sandstone along Interstate-35 between the Seward and Edmond exits in Oklahoma. Our quartz-cemented sandstone was purchased from Ward's Science. The limestone and sandstone were crushed and sieved, and the fraction collected between the US Standard sieves #7 and #10 (2.83 mm to 2 mm in diameter) was used. A subset of material from each of the rocks was gently powdered and analyzed via XRD to confirm the dominant mineralogy of each (Appendix A). These results indicated that the limestone used in these experiments was dominated by high-Mg calcite, the quartz-cemented sandstone contained a high level of quartz and minor amounts of clays, and that the mineralogy of the iron oxide-cemented sandstone was primarily quartz with clays and iron oxides consistent with US Geological Survey analysis of the

Garber Sandstone (Breit, 1991). The cementation of the Garber Sandstone is a combination of iron oxides and clays with varying amounts of each depending on the location; for this research, we will be referring to the cement of the Garber Sandstone as iron-oxide.

2.3 AMD Neutralization

All experiments were done in triplicate and contained 100 mL of AMD solution. Before and during the experiments, pH measurements were taken; after each pH measurement, the sample was shaken by hand to allow all surfaces of the grains to be exposed to the AMD. The duration of each experiment was 20 days, and the samples were continuously agitated on a MaxQ Shaker 2000 rotary shaker. After each experiment, 10 mL of the AMD solution was removed to evaluate the change in total and dissolved iron concentrations. Using Equation 13 and assuming an experimental volume of 100 mL, it was determined that 1.2 g of $CaCO_3$ would be required to neutralize the synthetic AMD. Additional experiments to investigate the impact of the mass of limestone (see Table 1) on the neutralization reaction were also conducted. For clarification, the term 'neutralization' is used in this work to refer to the AMD solution reaching a pH of ~7, with no consideration of the dissolved or total iron concentrations. As previously stated, each sample contained 100 mL of the AMD and placed on a shaker for 20 days. At select times during the experiment, the pH of each triplicate experiment was measured.

2.4 AMD Neutralization in the presence of limestone and sandstone

To investigate the impact of sandstone on the neutralization of AMD by limestone, replicate neutralization experiments were conducted. These experiments had a limestone to sandstone ratio of 1:1, with either 1.2 g or 0.6 g of limestone amended with an equal mass of either the iron oxide- or quartz-cemented sandstone with 100 mL of AMD. The limestone-sandstone batch experiments were periodically tested for pH as described above. Control

experiments containing only sandstone in 100 mL of AMD were conducted to verify that AMD neutralization was due to the dissolution of limestone. Table 1 provides details for each of the AMD neutralization reactions conducted.

Changes in iron speciation are an important factor in AMD neutralization; however, in the batch experiments described above, aqueous samples were not collected because doing so would have resulted in a continuously changing solid:solution ratio that would make interpreting the results more difficult. In light of this, a series of sacrificial experiments were conducted to investigate changes in the total and dissolved iron concentrations during AMD neutralization. The sacrificial experiments contained 40 mL of AMD and 0.96 g of solid material. After 5 hours, 12 hours, 24 hours, and 48 hours, the pH was measured, and 10 mL of solution was removed from each experiment with 5 mL unfiltered and 5 mL filtered. The unfiltered portion removed is the total iron concentration while the filtered portion is the dissolved iron concentration. The aqueous samples were analyzed using an Inductively Coupled Plasma Optical Emission Spectrometry (ICP-OES) to measure the amount of iron in the AMD after the exposure to the limestone and sandstone.

Table 1: Experimental Setup

Experiment Name:	Limestone: (g)	Iron Oxide-Cemented Sandstone: (g)	Quartz-Cemented Sandstone: (g)
LS(0.1)	0.1	0	0
LS(0.5)	0.5	0	0
LS(1.2)-A	1.2	0	0
LS(1.2)-B*	1.2	0	0
ISS	0	1.2	0
QSS	0	0	1.2
LS(0.6)+ISS-A	0.6	0.6	0
LS(0.6)+ISS-B	0.6	0.6	0
LS(0.6)+ISS*	1.2	1.2	0
LS(1.2)+QSS*	1.2	0	1.2

* Denotes experiments that were also sacrificial

2.5 Armoring and Iron Precipitates

At the conclusion of the QSS, LS(1.2)+QSS, ISS, and LS(1.2)+ISS experiments, the contents of each batch reactor was poured into weigh boats and were allowed to air-dry. Once dry, lithic grains were rinsed with distilled deionized water to remove any material that may have settled onto the grains during the drying process and air-dried again. Figure 4 shows the dried material recovered from experiments QSS, LS(1.2)+QSS, ISS, and LS(1.2)+ISS. The recovered materials include any limestone and sandstone grains as well as precipitates from the AMD solution. An Olympus BX50 microscope was used visually inspect limestone and sandstone grains for evidence of armoring at the conclusion of the neutralization experiments.

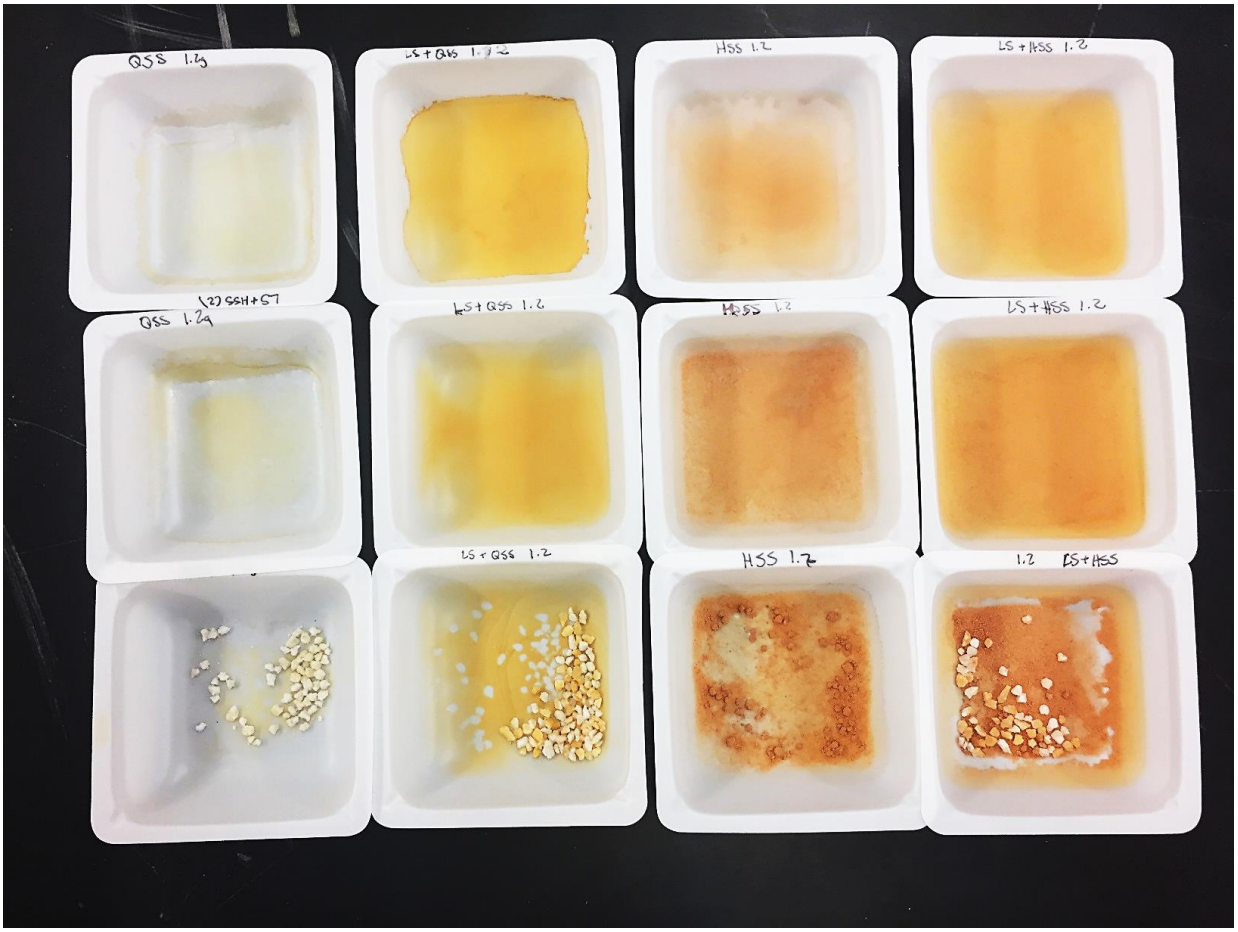

Figure 4: Each column contains the remaining material after the solution has evaporated. The first and second rows contain materials that were suspended in the AMD solution while the third row contains rock fragments. Starting from left to right: the first column is from QSS and contains quartz-cemented sandstone grains and minimal precipitates from the AMD; the second column is from LS+QSS and contains yellow precipitates from the AMD, limestone, and quartz-cemented sandstone grains; third column is from ISS and contains aggregated and disaggregated iron oxide-cemented sandstone fragments; the fourth column is from LS+ISS-3 and contains orange tinted precipitates from the AMD, limestone, aggregated and disaggregated iron oxide-cemented sandstone fragments.

III. RESULTS

3.1 Limestone and Sandstone Experiments

The initial pH of the AMD was 2.34, and Figure 5 compares the pH of the different amounts of limestone as a function of time. The LS(0.1) contained the 0.1g, LS(0.5) contained 0.5 g, and LS(1.2)-A contained 1.2 g of limestone. After 20 days, the pH for LS(1.2)-A reached a max of 7.16 and leveled out to 6.89, the pH for LS(0.5) reached a peak of 6.38, and the pH of LS(0.1) reached 2.50 (Figure 5). Because LS(1.2)-A is the only sample that reached neutralization (Figure 5), it was used as the amount of limestone for the rest of the experiments.

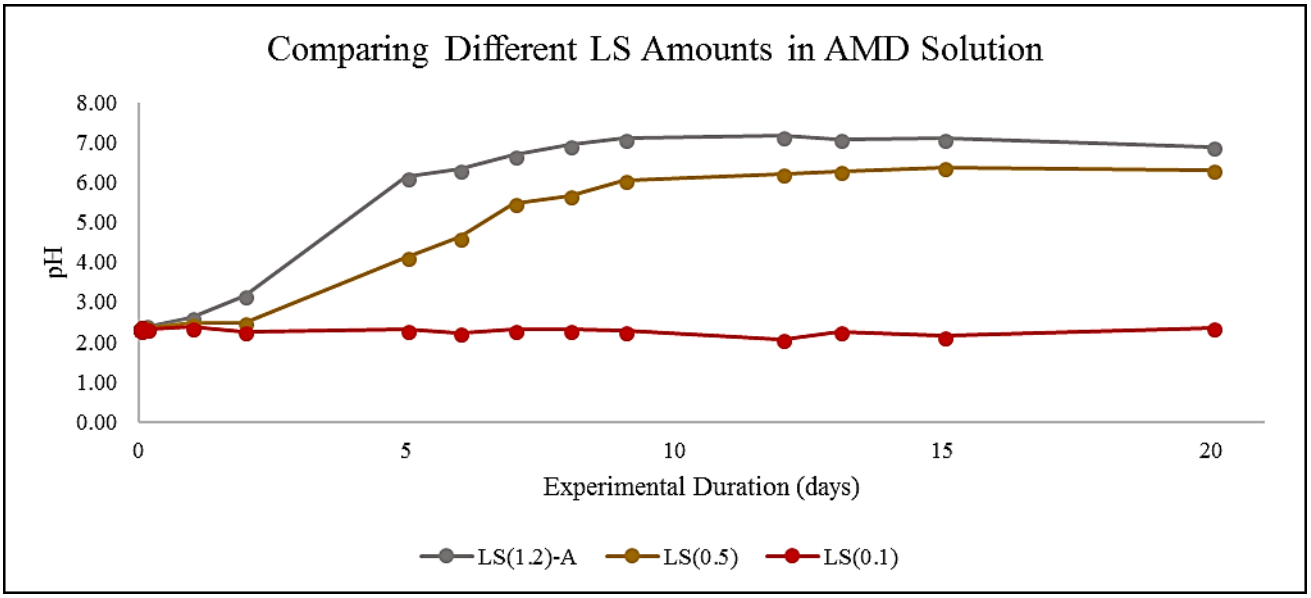

Figure 5: Plot of pH vs. experimental duration of LS(0.1), LS(0.5), and LS(1.2)-A in AMD soution.

The second limestone experiement, LS(1.2)-B, had an intial pH of 2.58 which is slightly higher than the orgianl AMD used in LS(1.2)-A. The neutralization occurred between 2 and 3 days and the final pH was 7.89 (Figure 6). The iron oxide-cemented sandstone (ISS) experiment and quartz-cemented sandstone (QSS) experiment had an initial pH of 2.72, and over the duration of 20 days, the pH value never surpassed 3 (Figure 6).

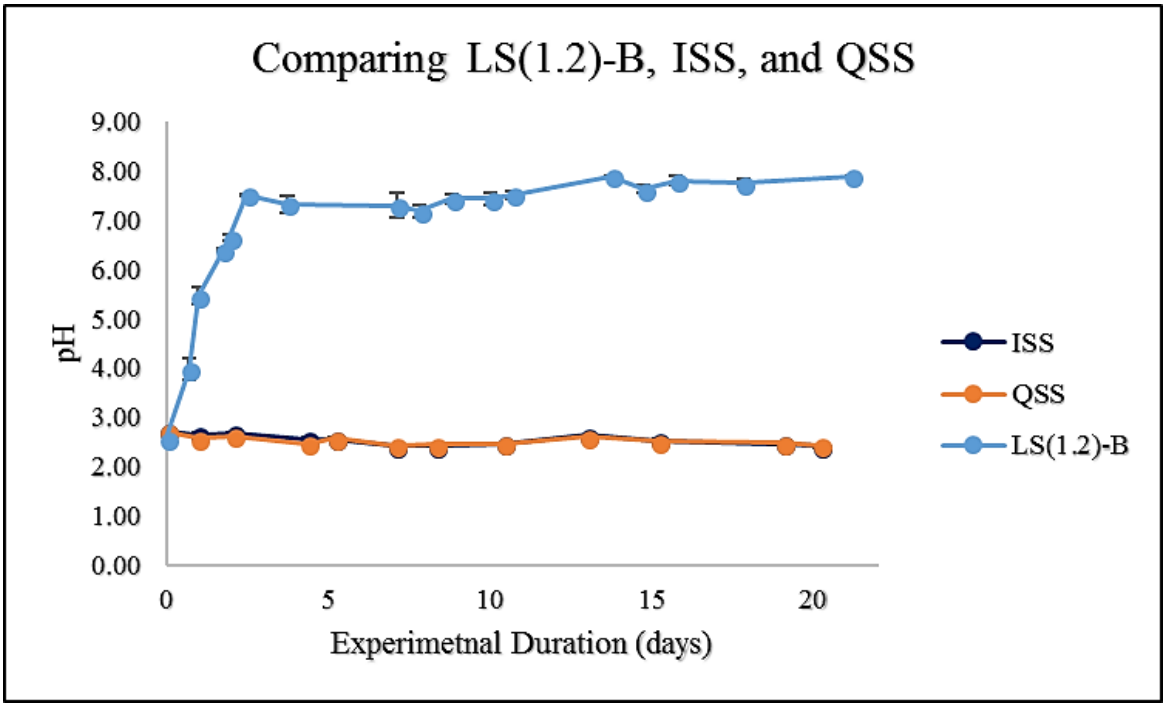

Figure 6: Plot of pH vs. experimental duration of LS(1.2)-B, ISS, and QSS. Error bars show standard errors from triplicate experiements.

3.2 Limestone and Iron Oxide-Cemented Sandstone Experiments

Experiment LS(0.6)+ISS-A contained 0.6 g of limestone and 0.6 g of iron oxide-cemented sandstone. The initial pH of the AMD was 2.18 and the final pH after 20 days was 7.15 (Figure 7) with neutralization occurring after 17 days. When comparing the neutralization of LS(1.2)-A and LS(0.6)+ISS-A, LS(0.6)+ISS-A did take longer to neutralize the AMD (Figure 7), which is not consistent with previous studies (Sasowsky et al., 2000). One possible explanation for this difference is that the initial pH of the AMD plays an important role in the initial rate of neutralization. LS(1.2) had a pH of 2.34 while the LS(0.6)+ISS-A had a pH of 2.18. At about a pH of 2.2, the dominant iron species changes from Fe^{3+} to $Fe(OH)^{2+}$ (Figure 3). The change in iron species could result in a change in solubility, releasing H^{+} into solution, which could be why the iron oxide-cemented sandstone hindered the neutralization. Another

explanation for the difference in results could be that the experiments had different masses of limestone (1.2 g vs. 0.6 g, see Table 1). Replicated experiments were conducted that used the same limestone masses but had the same initial AMD pH of 2.58 (LS(1.2)-B and LS(0.6)+ISS-B).

In the Limestone and Iron Oxide-Cemented Sandstone Experiment #2 (LS(0.6)+ISS-B), the initial pH of the AMD was 2.58 and the final pH was 7.93 (Figure 7). The neutralization occurred between 5 and 7 days. When comparing the results of LS(1.2)-B, LS(0.6)+ISS-A, and LS(0.6)+ISS-B, the results show that the addition of iron oxide-cemented sandstone does impact the neutralization of AMD (Figure 7). When comparing just LS(0.6)+ISS-A and LS(0.6)+ISS-B, the neutralization of the AMD in LS(0.6)+ISS-B occurred sooner by 13-10 days. The only difference between the two experiments is the initial pH, which varied by 0.4. A possible explanation could be that the iron chemistry changes depending on the initial pH of the AMD. To further investigate this issue, iron-sorption studies were conducted which are discussed later in the paper. However, regardless of the initial pH, the LS(1.2)-B reached neutralization quicker than the other experiments. LS(1.2)-B neutralized in 2-3 days while the LS(0.6)+ISS-A took 17 days and the LS(0.6)+ISS-B took 4-7 days. Even with the addition of sandstone and starting at the same initial pH, the neutralization of AMD was hindered. Now, the only difference between the experiments is the amount of limestone.

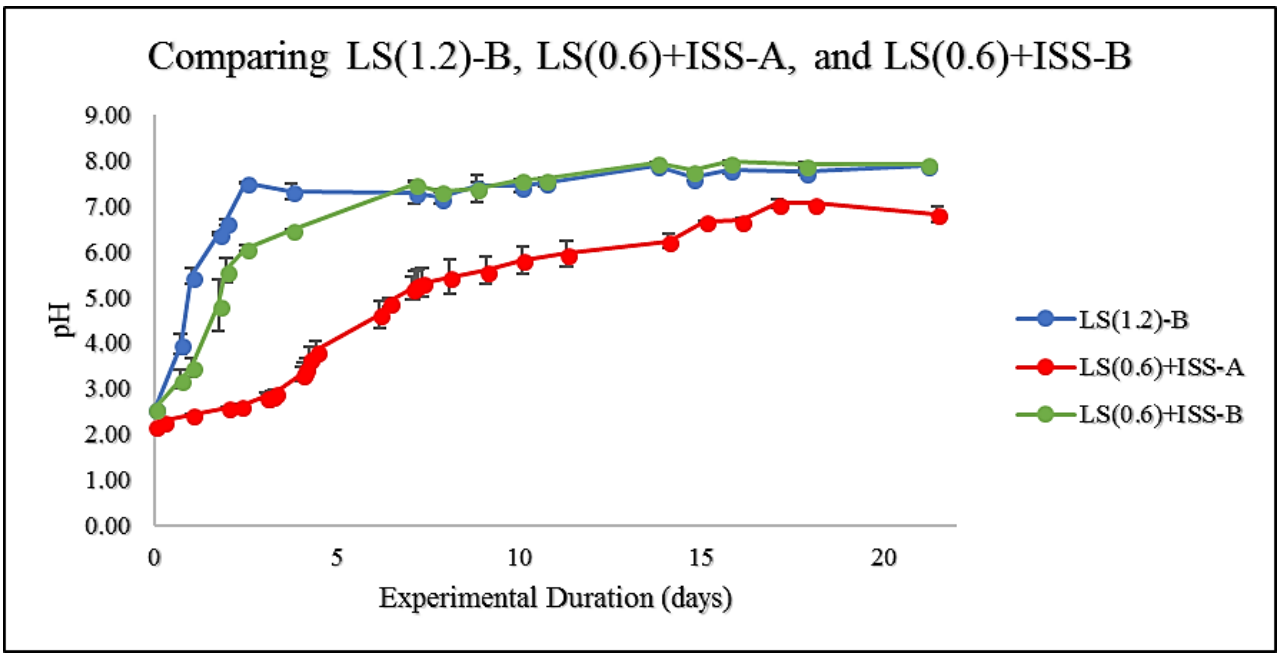

Figure 7: Plot of pH vs. experimental duration of LS(1.2)-B, LS(0.6)+ISS-A, and LS(0.6)+ISS-B. Error bars show standard errors from triplicate experiments.

In LS(1.2)-B there is 1.2 g of limestone while the other two experiments have 0.6 g of limestone. However, LS(0.6)+ISS-A and LS(0.6)+ISS-B only had 0.6 g. Figure 7 is a plot of pH over time for these experiments and clearly shows the amount of limestone present in the experiment played a dominant role in the amount of time required to neutralize the AMD.

Limestone and Iron Oxide-Cemented Sandstone Experiment #3, LS(1.2)+ISS, contained 1.2 g of limestone and 1.2 g of iron oxide-cemented sandstone. The initial pH of the AMD solution was 2.72, and the final pH was 7.32 (Figure 8). The AMD was neutralized after 4 days. When comparing LS(1.2)+ISS to the other experiments, the neutralization of the AMD occurred ~3 days sooner than the LS(0.6)+ISS-A and ~15 days sooner than LS(0.6)+ISS-B (Figure 8). These results are to be expected because the LS(1.2)+ISS has double the amount of limestone in LS(0.6)+ISS-A and LS(0.6)+ISS-B.

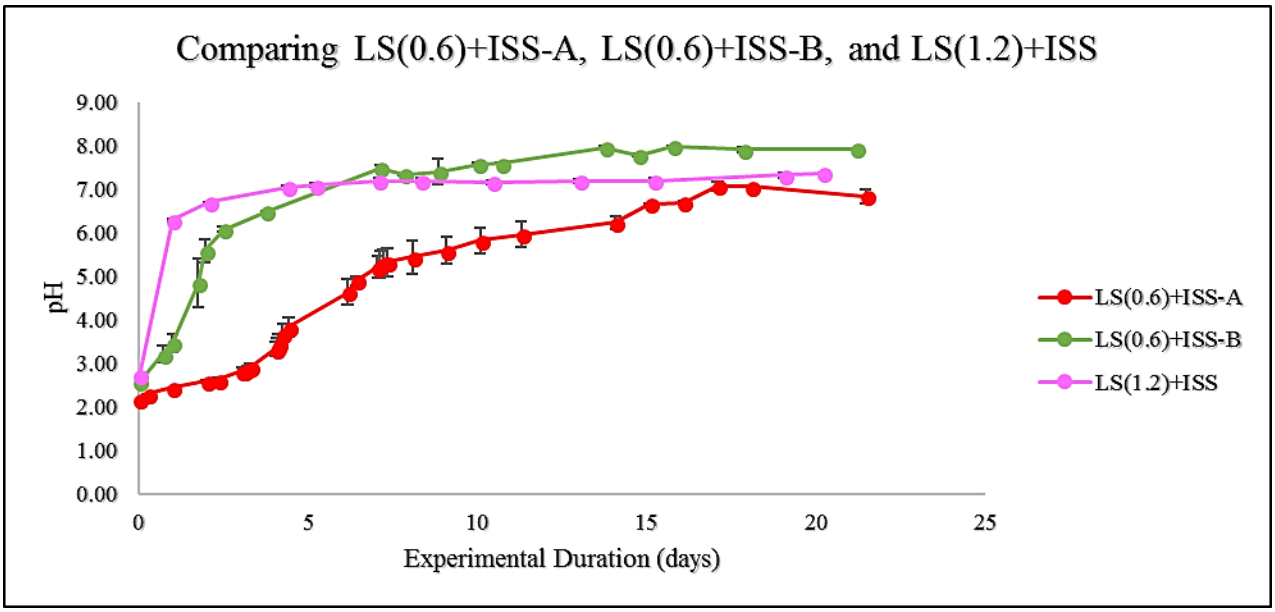

Figure 8: Plot of pH vs. experimental duration of LS(0.6)+ISS-A, LS(0.6)+ISS-B, and LS(1.2)+ISS. Error bars show standard errors from triplicate experiments.

3.3 Limestone and Quartz-Cemented Sandstone Experiment

The limestone and quartz-cemented sandstone (LS(1.2)+QSS) experiment contained 1.2 g of quartz-cemented sandstone and 1.2 g of limestone. The initial pH of the AMD was 2.72, the final pH was 7.40, and the AMD neutralized after 2 days (Figure 9). Comparing the LS(1.2)+QSS and LS(1.2)-B, the neutralization of the AMD occurred ~2 days earlier when the sandstone was present (Figure 9). In addition, after the first day, the pH of LS(1.2)+QSS was 6.69 while the pH of LS(1.2)-B was only 3.97 (Figure 9). As seen in Table 2, the main difference between these two experiments is the addition of the quartz-cemented sandstone. As seen in experiment QSS, the sandstone does not directly contribute to the neutralization process.

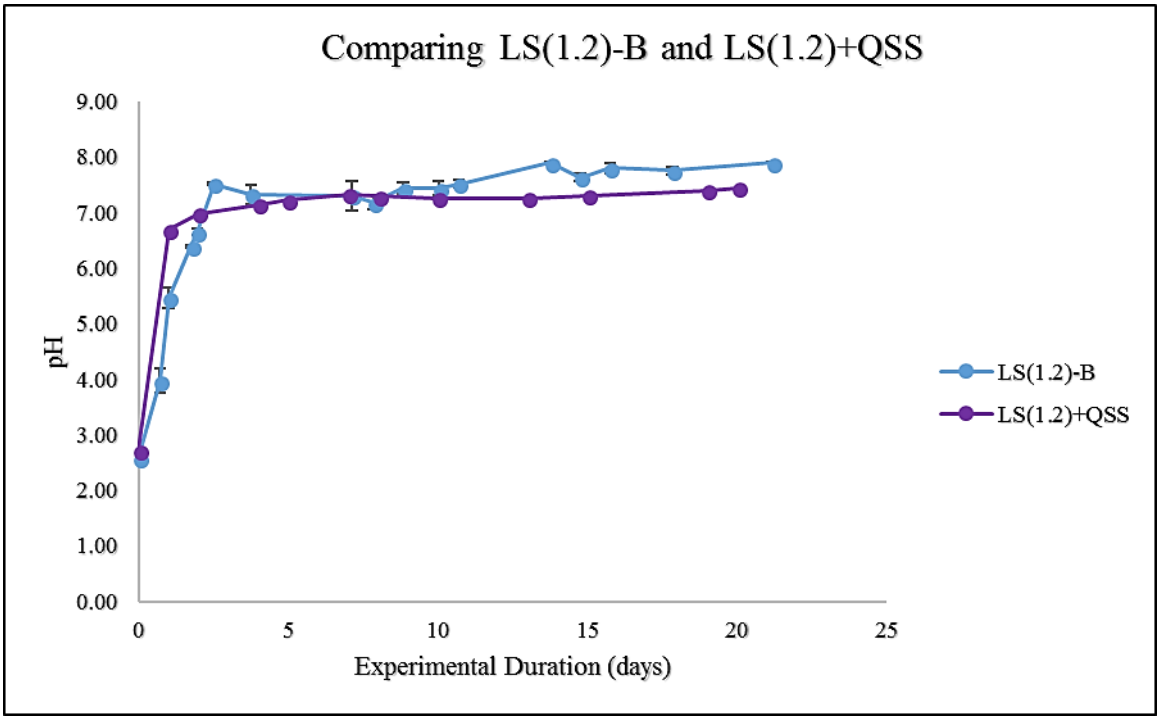

Figure 9: Plot of pH vs. experimental duration of LS(1.2)-B and LS(1.2)+QSS. Error bars show standard errors from triplicate experiments.

Table 2: Experiment Results

Experiment Name:	Initial pH:	Final pH:	Days Required to Reach Neutralization:
LS(0.1)	2.34	2.36	NA
LS(0.5)	2.34	6.31	NA
LS(1.2)	2.34	6.89	9
LS(1.2)-B*	2.58	7.89	3
ISS	2.72	2.53	NA
QSS	2.72	2.53	NA
LS(0.6)+ISS-A	2.18	6.83	17
LS(0.6)+ISS-B	2.58	7.93	~5
LS(1.2)+ISS*	2.72	7.36	~3
LS(1.2)+QSS*	2.72	7.45	2

* Denotes experiment were also sacrificial

3.4 Sacrificial Replicant Experiments

The sacrificial experiments were replicants of LS(1.2)-B, LS(1.2)+ISS, and LS(1.2)+QSS. The sacrificial replicant experiments contained 0.96 g of solid and 40 mL of AMD solution. The LS(1.2)-B replicant experiment contained 0.96 g of limestone only, while

the other sacrificial replicant experiments contained 0.48 g of limestone and 0.48 g of sandstone. The starting total iron concentration was 57.35 ppm and dissolved iron concentration was 11.83 ppm for all the sacrificial replicant experiments. In all of the sacrificial replicant experiments, the dissolved iron concentration decreased to ~0 ppm within 5 hours and remained there for the duration of the experiment (Figures 10, 11, 12). This is to be expected because as the pH of the AMD solution goes towards neutralization, the dissolved iron in the AMD precipitates out of solution. In the limestone sacrificial experiment, the total iron decreased to ~34 ppm after 12 hours, followed by an increase to ~46 ppm after 24 hours; the final concentration was ~38 ppm (Figure 10). In the iron oxide-cemented sandstone sacrificial experiment, the total iron concentration decreased to ~45 ppm after 12 hours, then increased to ~48 ppm after 24 hours; the final concentration was ~45 ppm (Figure 11). In the quartz-cemented sandstone sacrificial experiment, the total iron concentration decreased to ~40 ppm after 5 hours, then increased to ~47 ppm after 12 hours; after 24 hours, the total iron concentration decreased to ~41 ppm, then increased to ~51 ppm (Figure 11). With all the sacrificial experiments, the total iron concentration decreased which is expected to happen as the iron precipitates out of solution. The total iron concentration also decreased over the duration of the experiments, which is consistent with precipitation and surface adsorption of iron oxides. However, the total iron concentrations at the end of the experiments indicate that a considerable amount of suspended colloidal iron is still present.

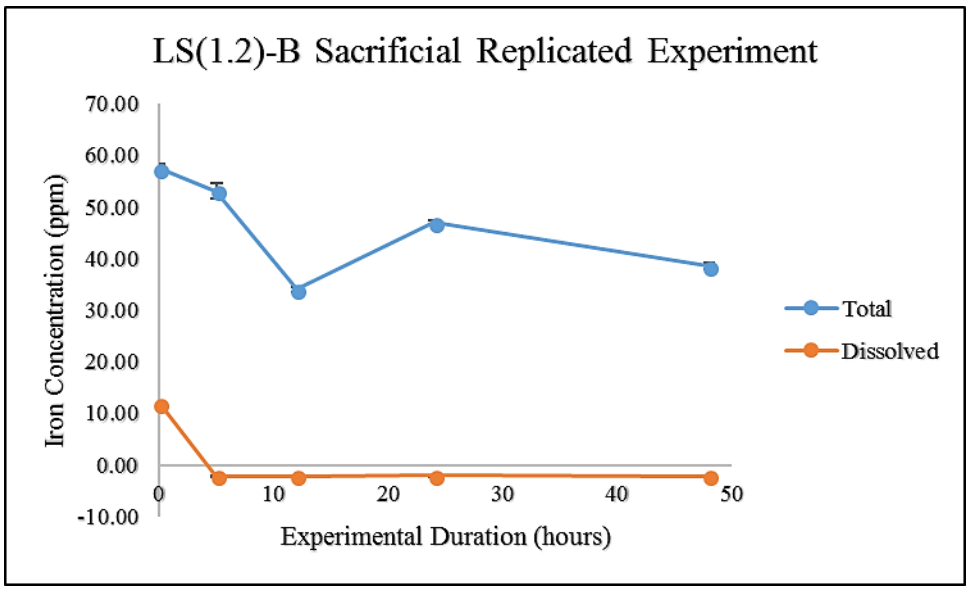

Figure 10: Plot of total and dissolve iron concentration vs experimental duration in the LS(1.2)-B sacrificial replicated experiment. Error bars show standard errors from triplicate readings.

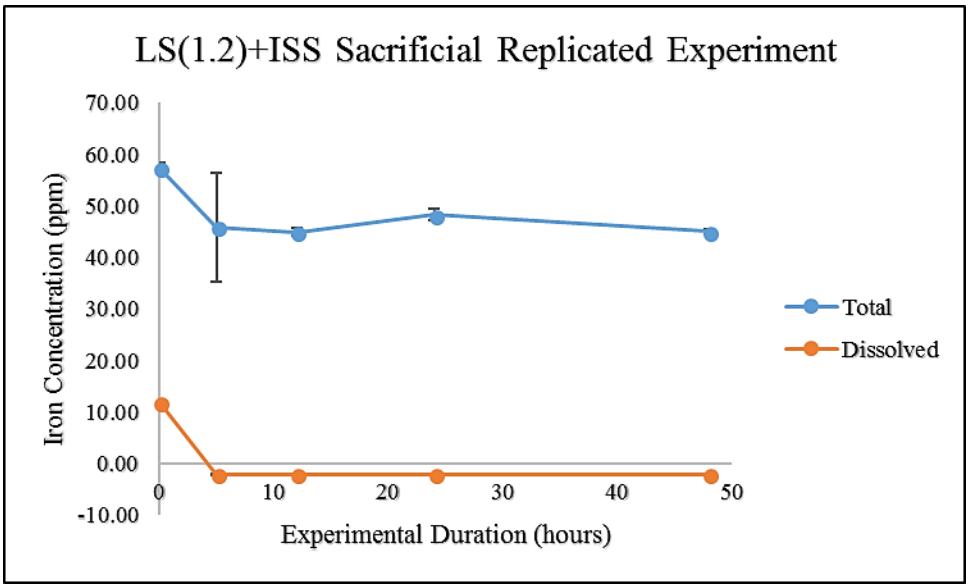

Figure 11: Plot of total and dissolve iron concentration vs. experimental duration in the LS(1.2)+ISS sacrificial replicated experiment. Error bars show standard errors from triplicate readings.

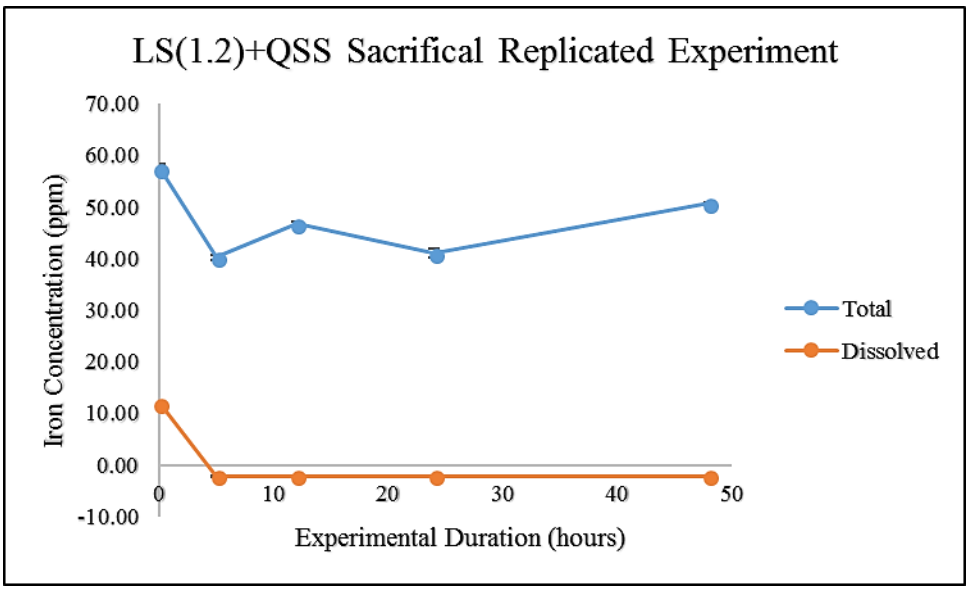

Figure 12: Plot of total and dissolve iron concentration vs. experimental duration in the LS(1.2)+QSS sacrificial replicated experiment. Error bars show standard errors from triplicate readings.

3.5 Armoring of grains

Figure 13 shows limestone and quartz-cemented sandstone grains before and after exposure to AMD. The images clearly show that both limestone and sandstone grains were subjected to armoring during the AMD neutralization reaction. Figure 14 shows a representative sample from LS(1.2)-B and Figure 15 shows a representative sample from LS(1.2)+QSS. In the LS(0.6)+ISS-B experiment, the iron-oxide cemented sandstone grains disaggregated during the experiment, therefore, microscope photographs were unable to be obtained. As seen in Figure 14, there are 27 limestone grains from LS(1.2)-B, which 18 are armored and 9 are not armored. In total, ~66% of the grains are armored while ~34% are not. When viewing the grains from LS(1.2)+QSS, the quartz-cemented sandstone grains had more armoring than the limestone grains (Figure 15). In Figure 16, there are 39 grains from LS(1.2)+QSS with 16 of them being limestone and 23 are quartz-cemented sandstone. Out of the 16 limestone grains, 6 are armored or 36%. Out of the 23 quartz-cemented sandstone grains, 17 are armored or 74%. From this representative sample, there are twice as many armored quartz-cemented sandstone grains than

armored limestone grains. When comparing the percentage of armored limestone from LS(1.2)-B and LS(1.2)+QSS, there is ~31% decrease in the number of armored limestone grains.

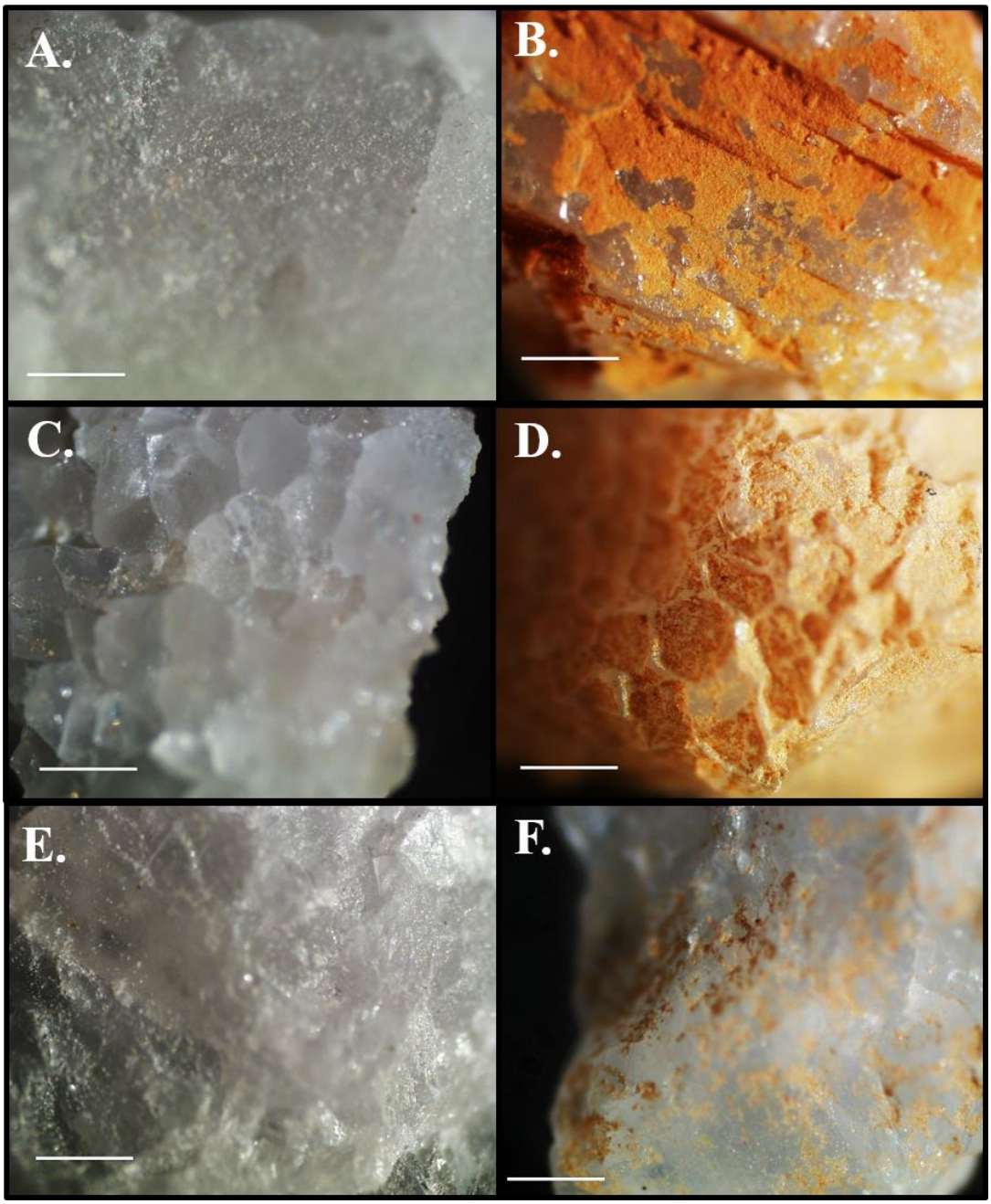

Figure 13: Images collected under a light microscope 10x. Scale bar is 1 mm in all images. A) A limestone grain prior to AMD exposure. B) A limestone grain armored in iron precipitates from LS(1.2)-B. C) A quartz-cemented sandstone grain prior to AMD exposure. D) A quartz-cemented sandstone grain armored in iron precipitates from LS(1.2)+QSS. E) A limestone grain prior to AMD exposure. F) A limestone grain armored in iron precipitates from LS(1.2)+QSS.

Figure 14: A representative sample of limestone grains from the experiment LS(1.2)-B. The orange color is from the armoring of iron precipitates. Scale bar is 2 mm.

Figure 15: Representative grains from the LS(1.2)+QSS experiment. The top grains are the quartz-cemented sandstone and the grains at the bottom of the photograph are limestone. The orange color is from the armoring of iron precipitates. Scale bar is 2 mm.

IV. DISCUSSION

4.1 Neutralization of AMD

Experimental results show that the neutralization of AMD comes from the dissolution of carbonate in the limestone and that non-carbonate bearing sandstone does not act to neutralize AMD. These results are consistent with Xu et al. (1997) who reported that sandstone with no calcium carbonate could not neutralize the AMD. Additionally, experimental results showed that the mass of reactive limestone was a key variable in the neutralization of AMD. The synthetic AMD was not neutralized in the experiments that contained less than 1.2 g of limestone, which was the minimum amount calculated to be needed for neutralization. When limestone was present at a mass of 1.2 g, neutralization was relatively rapid in most of the experiments in this investigation. These results contrasts with those of Santomartino and Webb (2007), who reported that during AMD neutralization, a maximum pH of 6.45 was achieved before the pH gradually decreased to below 6 after 150 hours due to the armoring of the limestone. The differing results can be attributed to the difference in experimental set-up. Santomartino and Webb (2007) used a small-scale limestone system consisting of a column filled with limestone gravel and had synthetic AMD pumped through at 2.75 mL per minute, so that during the experiment the limestone was continuously exposed to fresh AMD. This work used continuously agitated batch reactors. Based on their stated methods, Santomartino and Webb (2007) had excess of limestone present in their experiments, which would have been sufficient to neutralize the synthetic AMD. However, the continuous flow set-up by Santomartino and Webb (2007) subjected the limestone to a continuous supply of dissolved iron, which allowed for a greater accumulation iron precipitates on the limestone grains, inhibiting further neutralization.

In experiments LS(0.6)+ISS-B and LS(1.2)+ISS, the only difference in the experiments was the amount of limestone (Table 1, 2); therefore, the difference for when neutralization occurred is due to the amount of limestone (Figure 16). As stated previously, limestone provides the means for neutralization through the dissolution of carbonate; therefore, the experiment with less limestone would not have the same neutralization rate as one with more limestone. In Iakovelva et al. (2015) reported that 50 g of limestone neutralized the AMD sooner than the 20 g of limestone. Since LS(1.2)+ISS had more limestone, the neutralization of the AMD should have occurred sooner, which it did.

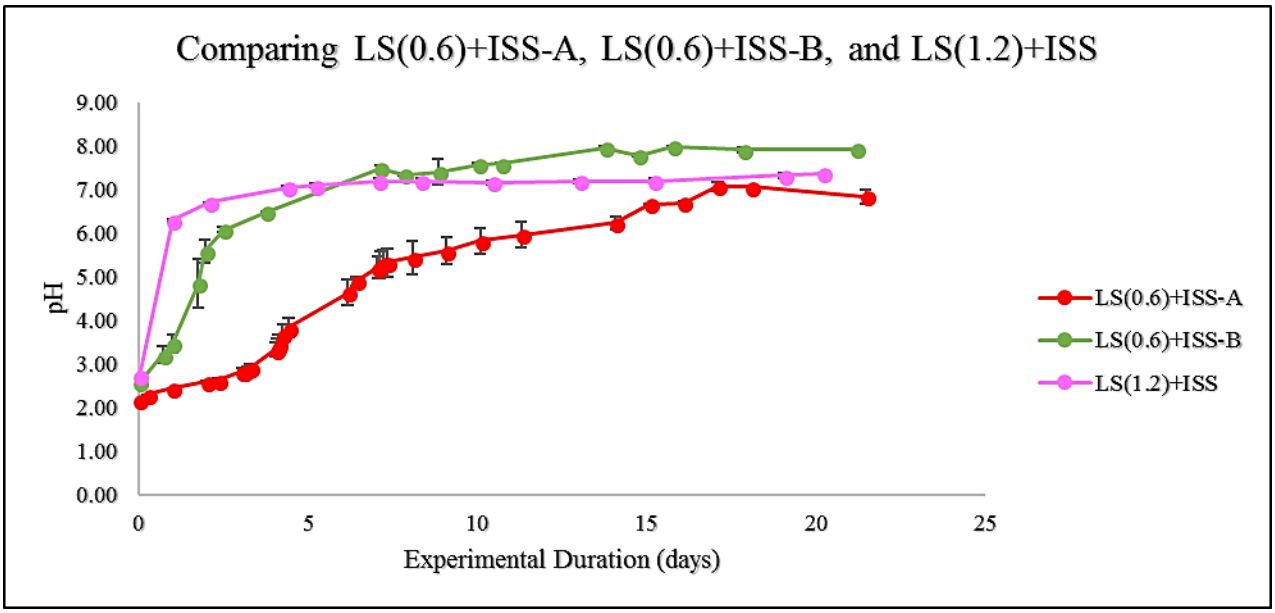

Figure 16: Plot of pH vs. experimental duration of LS(0.6)+ISS-B and LS(1.2)+ISS. Error bars show standard errors from triplicate experiments.

Experimental results also showed that the initial pH of the synthetic AMD played a role in the limestone-AMD neutralization reaction. The data in Table 2 clearly shows that as the initial pH of the synthetic AMD decreases from 2.52 to 2.18 in the LS+ISS experiments, the time required to reach a neutralization pH (~7) increases from ~5 days to ~17 days. This difference may be attributable to the speciation of iron at those initial pH values (Figure 17). Between the pH of 2.18 and 2.58, a critical change in the iron chemistry is impacting the neutralization rate.

Zhu et al. (2012) reported that in AMD under an initial pH of 2.2, ferric iron sulfate solutions form sulfate-complexed ferrihydrite-like molecular clusters. However, at an initial pH of ~2.5, those ferrihydrite-like clusters then gradually converted to schwertmannite, which is a more stable structure. When the pH was increased to an initial value of ~2.7, the ferrihydrite-like clusters immediately converted to schwertmannite (Zhu et al., 2012). The conversion of the ferrihydrite-like clusters into more stable forms releases H^+, which offsets the uptake of H^+ by the carbonate; thus, slowing down the neutralization rate until all of the ferrihydrite-like clusters are removed by the system. No mineralogical analysis of the colloidal iron was attempted as part of this work; however, the neutralization experiments indicate that a mechanism similar to that proposed by Zhu et al. (2012) impacted the pH in these experiments. In LS(0.6)+ISS-A and LS(0.5), the initial pH was below ~2.3, while in LS(0.6)+ISS-B, the initial pH was ~2.6. These experiments all had similar amounts of limestone (~0.5-0.6 grams), yet had very different neutralization curves (Figure 17). It is likely that at pH <~2.3 (LS(0.5) and LS(0.6)+ISS-A), the conversion of suspended iron to more stable forms was a slower process, resulting in a relatively prolonged release of H^+, which hindered neutralization. This process also occurred in the experiments with a higher pH (e.g. LS(0.6)+ISS-B); however, the initial pH of ~2.6 closer to the threshold of ~2.7, so the conversion of the suspended iron would have occurred more rapidly, effectively removing that particular buffering mechanism from the system and allowing pH to rise faster relative to the experiments with the lower initial pH.

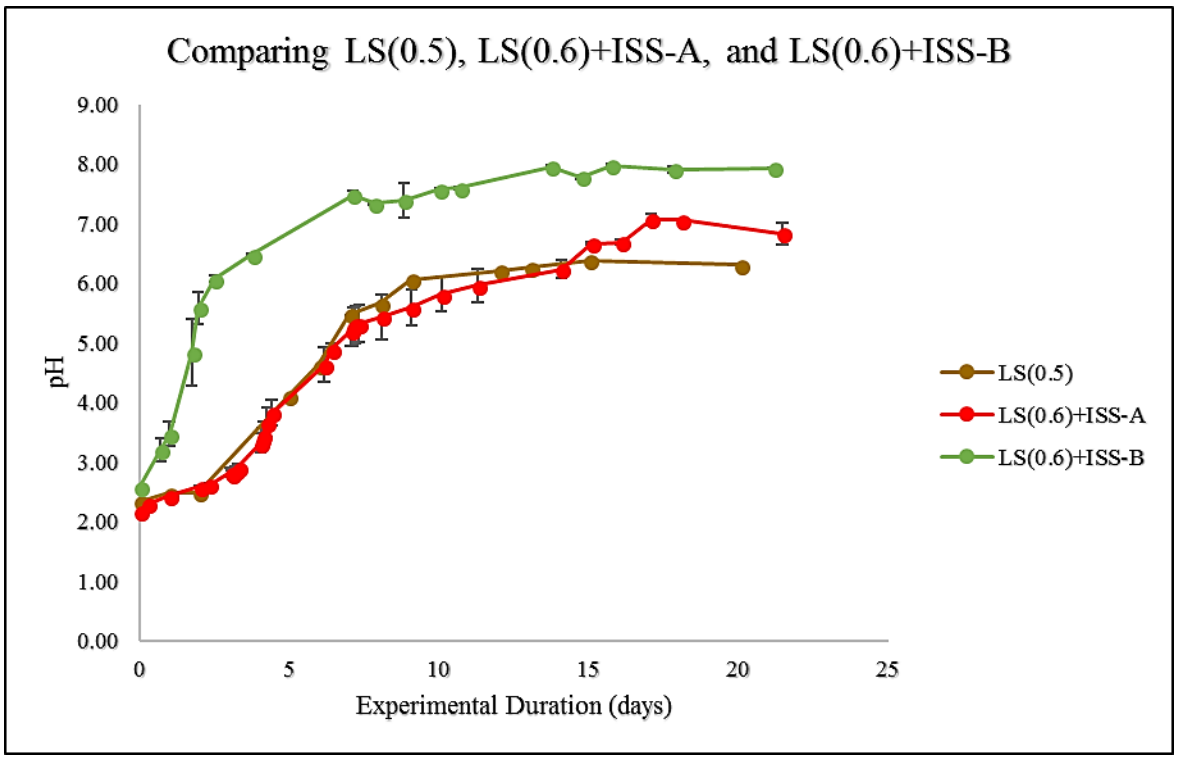

Figure 17: Plot of pH vs. experimental duration of LS(0.5), LS(0.6)+ISS-A, and LS(0.6)+ISS-B. Error bars show standard errors from triplicate experiments.

4.2 Limestone Armoring

Experimental results showed that when sufficient limestone is present to neutralize AMD, the addition of sandstone to the experiments slightly increased the rate of neutralization (Figure 18). In experiment LS(1.2)-B took ~3 days, while the neutralization for the LS(1.2)+ISS and LS(1.2)+QSS took ~2 days. Neutralization occurred sooner in experiments with sandstone because the iron oxide precipitates preferentially armored the sandstone, which decreased the rate of armoring of the limestone; allowing for a greater amount of carbonate dissolution to occur. Similarly, experiments LS(0.5) and LS(0.6)+ISS-A both had insufficient limestone to completely neutralize the synthetic AMD based on our calculations. However, LS(0.6)+ISS-A reached neutralization while LS(0.5) did not, likely due to the presence of sandstone in the former experiment, which inhibited the armoring of the limestone grains allowing for the neutralization reaction to continue.

The preferential armoring of the sandstone is likely due to the differences in the mineralogy of the lithic material. Every mineral surface has a point where the total concentration of surface anion sites is equal to the total concentration of surface cation sites, known as the point of zero charge (pH_{pzc}). When the pH is below pH_{pzc}, there is a net positive surface charge, and when the pH is above pH_{pzc}, there is a net negative surface charge. In low pH water, such as AMD, the precipitated iron oxides have a positive surface charge (Brady and Weil, 2008; Cornell, 2006; Stumm and Sulzberger, 1992). The limestone has a pH_{pzc} of 8 to 9 (Somasundaran and Agar, 1967), the quartz-cemented sandstone has a pH_{pzc} of 1.5 to 3.5 (Jada et al., 2006; Noh and Schwarz, 1989; Schwarz et al., 1984), and pH_{pzc} of the iron oxide-cemented sandstone is about 6 (Sumner, 1963). This means that between the pH values 3.5 and 6, the precipitated iron oxides will be attracted to the quartz since it has a negative surface change, and once the pH reaches 6, the iron oxide-cemented sandstone will have a negative surface charge. Because the quartz- and iron oxide-cemented sandstones have lower pH_{pzc}, the precipitated iron oxides will be preferentially attracted to those rather than the limestone, resulting in a quicker neutralization of AMD. Sasowsky et al. (2000) observed that the precipitated iron oxides were preferentially adsorbing onto sandstone rather than limestone; decreasing armoring of the limestone. The author attributed the preferential adsorption onto sandstone to its more negative surface charge relative to the limestone. While the pH_{pzc} of the lithic material used in this work was not determined, results of these experiments indicate that sandstone fragments are preferentially armored during the neutralization of AMD, consistent with the results of Sasowsky et al. (2000).

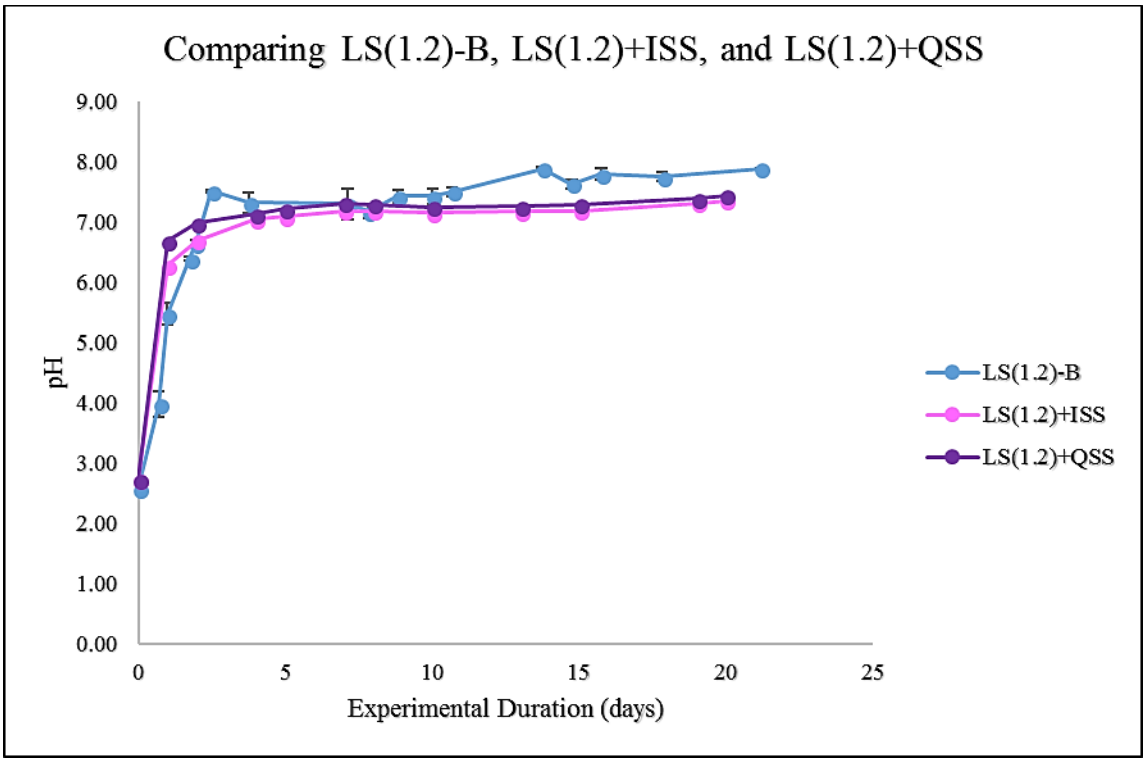

Figure 18: Plot of pH vs. experimental duration of LS(1.2)-B, LS(1.2)+ISS, and LS(1.2)+QSS. Error bars show standard errors from triplicate experiments.

4.3 Impact of flow regime on AMD neutralization

Sacrificial neutralization experiments were paired with replicated batch experiments to ensure that the neutralization process was reflective of what had been observed in the previous batch experiments. However, the pH neutralization trend in the first set of sacrificial experiments was notably different from the equivalent batch experiments. As seen in Figure 19, the initial sacrificial experiments took more than a week to reach a pH of ~7, whereas the corresponding batch reactors reached the same pH in about 2 days. While these experiments varied in scale, the solid:solution ratios were identical, so the neutralization trends were expected to be similar. However, the initial sacrificial experiments used centrifuge tubes with a conical base while the larger batch reactors were rectangular containers with a flat base. It was hypothesized that the shape of the container was impacting the flow dynamics by allowing the rock fragments to aggregate in the cone of the tube and preventing thorough h mixing with the

AMD. To test this hypothesis, a second set of sacrificial experiments was conducted using the containers with the flat base. Figure 20 shows the results of the second set of sacrificial experiments, and clearly indicates that the neutralization trend is similar to that of the corresponding batch neutralization reactions, although the greater pH measurement interval in the batch reactors makes comparisons during the 1-20 hour interval difficult. Taken together, these results indicate that the flow regime is an important factor in the AMD neutralization process. Ziemkiewicz et al. (1997) reported that the slope of an open limestone trench plays a critical role in the neutralization and armoring processes. The author concluded that slopes with a 1-3% incline would have inefficient neutralization due to heavy armoring while slopes with a 40% or greater incline resulted in neutralization and less armoring of the limestone. As the gradient of the slope is increased, the amount of time the AMD is in contact with the limestone is decreased. However, the increase in gradient results in more turbulent flow, which not only results in greater mixing of the AMD, but also acts to keep iron colloids in suspension, preventing these materials from accumulating on the surface of the limestone fragments. It is likely that the mixing regime in the different sacrificial experiments is responsible for the different sacrificial experiments is responsible for the different neutralization trends in what are otherwise identical experiments.

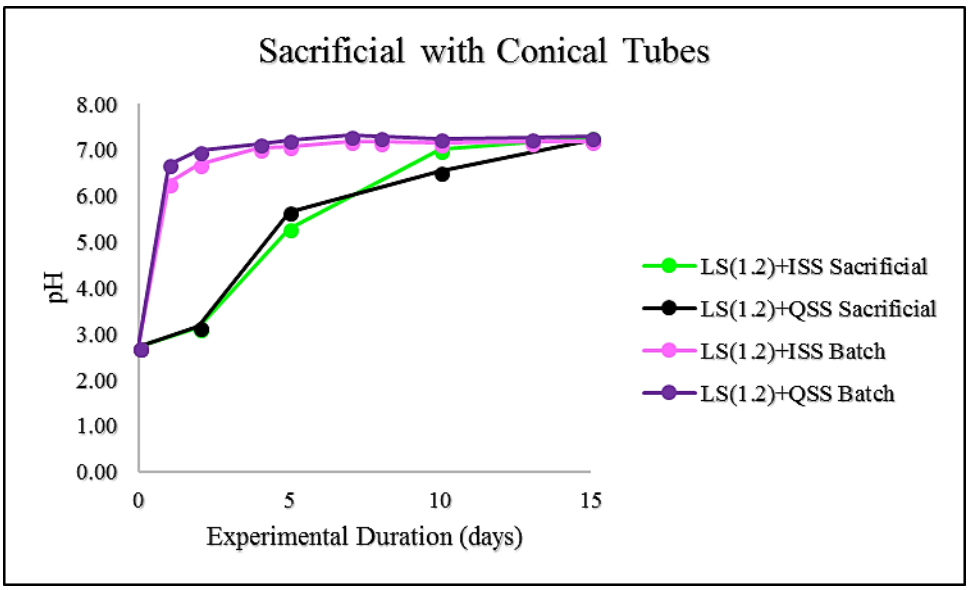

Figure 19: Plot of pH vs. experimental duration of the sacrificial replicated experiments in conical shaped test tubes.

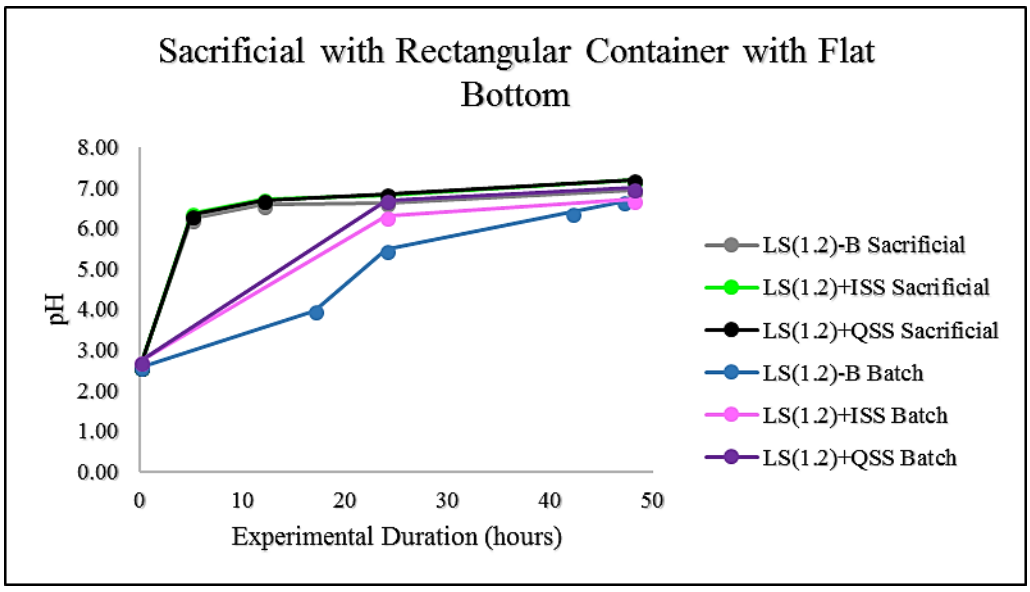

Figure 20: Plot of pH vs. experimental duration of the sacrificial replicated experiments in rectangular container with a flat bottom.

V. CONCLUSIONS

In the experiments conducted in this research, the data suggests that the rate of neutralization of AMD is impacted by several factors such as the initial pH, experimental set-up, and the amount of limestone. The goal of this research was to determine if the presence of sandstone effects the armoring of limestone during the AMD neutralization reaction, and if the mineralogy of the sandstone plays a role in this reaction. Experimental data suggest that the addition of sandstone may increase the ability of limestone to neutralize AMD due to the iron precipitates preferentially armoring the sandstone rather than the limestone, although the current results indicate that the increase is small. Additionally, quartz-cemented sandstone had a slightly greater impact on the neutralization reaction than did iron oxide-cemented sandstone. While adding sandstone did reduce the armoring of limestone, the mass of limestone present was a more important factor in the neutralization of AMD. However, when the overall results of this work are considered in light of the work of others (Iakovleva et al., 2015; Santomartino and Webb, 2007; Sasowsky et al., 2000; Xu et al., 1997; Zhu et al., 2012; Ziemkiewicz et al., 1997) it becomes apparent that the experimental set-up critically impacts the neutralization reaction. The chemistry of the AMD and the presence of organic matter will have a significant impact on the formation of colloidal materials as the pH of the AMD changes. Additionally, in a passive limestone trench, the flow regime will play a critical role in retention and settling of AMD precipitates, which significantly impacts the degree to which the limestone in the trench is armored. This underscores the need for additional work on the neutralization of AMD in passive limestone trenches using an experimental set-up that more closely resembles the continual flow of fresh AMD that would be encountered in an actual remediation system.

BIBLIOGRAPHY

BIBLIOGRAPHY

Akcil, A., and Koldas, S., 2006, Acid Mine Drainage (AMD): Causes, Treatment and Case Studies: Journal of Cleaner Production, no. 14, p. 1139-1145.

Baker, B. J., and Banfield, J. F., 2003, Microbial Communities in Acid Mine Drainage: The Federation of European Microbiological Societies (FEMS) Microbiology Ecology, no. 44, p. 139-152.

Barnes, H. L., and Romberger, S. B., 1968, Chemical Aspects of Acid Mine Drainage: Water Pollution Control Federation, v. 40, no. 3, p. 371-384.

Benner, S. G., Gould, W. D., and Blowes, D. W., 2000, Microbial populations associated with the generation and treatment of acid mine drainage: Chemical Geology, v. 169, no. 3–4, p. 435-448.

Berger, A., Gier, S., and Krois, P., 2009, Porosity-preserving chlorite cements in shallow-marine volcaniclastic sandstones: Evidence from Cretaceous sandstones of the Sawan gas field, Pakistan: AAPG Bulletin, v. 93, no. 5, p. 595-615.

Berner, R. A., 1970, Sedimentary pyrite formation: American Journal of Science, v. 268, no. 1, p. 1-23.

Brady, N. C., and Weil, R. R., 2008, The nature and properties of soils, Upper Saddle River, N.J., Pearson Prentice Hall.

Breit, G. N., 1991, Mineralogy and petrography of Permian rocks in the Central Oklahoma aquifer, [Denver, CO] :, U.S. Dept. of the Interior, Geological Survey, Open-file report / U.S. Geological Survey ; 90-678; Open-file report (Geological Survey (U.S.)) ; 90-678.

Burke, S. P., and Banwart, S. A., 2002, A geochemical model for removal of iron(II)(aq) from mine water discharges: Applied Geochemistry, v. 17, no. 4, p. 431-443.

Burley, S. D., and Worden, R. H., 2003, Sandstone diagenesis : recent and ancient, Malden, MA, Malden, MA : Blackwell Pub.

Cornell, R. M., 2006, The Iron Oxides Structure, Properties, Reactions, Occurrences and Uses, Hoboken, Hoboken : Wiley, The Iron Oxides - Structure, Properties, Reactions, Occurences and Uses.

Cravotta Iii, C. A., and Trahan, M. K., 1999, Limestone drains to increase pH and remove dissolved metals from acidic mine drainage: Applied Geochemistry, v. 14, no. 5, p. 581-606.

Department of Energy, U. S., A Brief History of Coal Use, Volume 2017.

Department of Interior, U. S., Volume 2017.

Evangelou, V. P., 1995, A Review- Pyrite Oxidation Mechanisms and Acid-Mine Drainage Prevention: Critical reviews in environmental science and technology, v. 25, no. 2, p. 141-199.

García, C., Moreno, D. A., Ballester, A., Blázquez, M. L., and González, F., 2001, Bioremediation of an industrial acid mine water by metal-tolerant sulphate-reducing bacteria: Minerals Engineering, v. 14, no. 9, p. 997-1008.

Gazea, B., Adam, K., and Kontopoulus, A., 1995, A Review of Passive Systems for the Treatment of Acid Mine Drainage: Minerals Engineering, v. 9, no. 1, p. 23-42.

Gibert, O., de Pablo, J., Luis Cortina, J., and Ayora, C., 2004, Chemical characterisation of natural organic substrates for biological mitigation of acid mine drainage: Water Research, v. 38, no. 19, p. 4186-4196.

Gray, N. F., 1997, Environmental impact and remediation of acid mine drainage: a management problem: Environmental Geology, v. 30, no. 1/2, p. 62-71.

Hedin, R. S., Watzlaf, G. R., and Nairn, R. W., 1994, Passive Treatment Of Acid Mine Draiange with Limestone: Journal of Environmental Quality, v. 23, p. 1338-1345.

Iakovleva, E., Makila, E., Salonen, J., Sitarz, M., and Wang, S., 2015, Acid Mine Drainage (AMD) Treatment: Neutralization And Toxic Elements Removal With Unmodified And Modified Limestone: Ecological Engineering, v. 81, p. 30-40.

Jada, A., Ait Akbour, R., and Douch, J., 2006, Surface charge and adsorption from water onto quartz sand of humic acid: Chemosphere, v. 64, no. 8, p. 1287-1295.

Johnson, D. B., and Hallberg, K. B., 2005, Acid Mine Drainage Remediation Options: A Review: Science of the Total Environment, no. 338, p. 3-14.

Kairies, C. L., Capo, R. C., and Watzlaf, G. R., 2005, Chemical and physical properties of iron hydroxide precipitates associated with passively treated coal mine drainage in the Bituminous Region of Pennsylvania and Maryland: Applied Geochemistry, v. 20, no. 8, p. 1445-1460.

Kaksonen, A. H., and Puhakka, J. A., 2007, Sulfate Reduction Based Bioprocesses for the Treatment of Acid Mine Drainage and the Recovery of Metals: Engineering in Life Sciences, v. 7, no. 6, p. 541-564.

Lower, S., 2017, General Chemistry, LibreTexts.

McCauley, C. A., O'Sullivan, A. D., Milke, M. W., Weber, P. A., and Trumm, D. A., 2009, Sulfate and metal removal in bioreactors treating acid mine drainage dominated with iron and aluminum: Water Research, v. 43, no. 4, p. 961-970.

Neculita, C.-M., Zagury, G. J., and Bussière, B., 2007, Passive Treatment of Acid Mine Drainage in Bioreactors using Sulfate-Reducing Bacteria: Journal of Environmental Quality, v. 36, no. 1, p. 1-16.

Noh, J. S., and Schwarz, J. A., 1989, Estimation of the point of zero charge of simple oxides by mass titration: Journal of Colloid and Interface Science, v. 130, no. 1, p. 157-164.

Nordstrom, D. K., Bowell, R. J., Campbell, K. M., and Aplers, C. N., 2017, Challenges in Recovering Resources from Acid Mine Drainage: Mine Water and Circular Economy, v. 2.

Ole, e., Timothy David, C., and Kaj, e.-J., 2013, Underwater photosynthesis of submerged plants – recent advances and methods: Frontiers in Plant Science, Vol 4 (2013).

Pyzik, A. J., and Sommer, S. E., 1981, Sedimentary iron monosulfides: Kinetics and mechanism of formation: Geochimica et Cosmochimica Acta, v. 45, no. 5, p. 687-698.

Robb, G. A., and Robinson, J. D. F., 1995, Acid Drainage from Mines: The Geographical Journal, v. 161, no. 1, p. 47-54.

Rose, S., and Elliott, W. C., 2000, The effects of pH regulation upon the release of sulfate from ferric precipitates formed in acid mine drainage: Applied Geochemistry, v. 15, no. 1, p. 27-34.

Santomartino, S., and Webb, J. A., 2007, Estimating the longevity of limestone drains in treating acid mine drainage containing high concentrations of iron: Applied Geochemistry, v. 22, no. 11, p. 2344-2361.

Sasowsky, I. D., Foos, A., and Miller, C. M., 2000, Lithic Controls On The Removal Of Iron And Remediation Of Acid Mine Drainage: Water Resources, v. 34, no. 10, p. 2742-2746.

Schwarz, J. A., Driscoll, C. T., and Bhanot, A. K., 1984, The zero point of charge of silica—alumina oxide suspensions: Journal of Colloid and Interface Science, v. 97, no. 1, p. 55-61.

Skousen, J. G., and Foreman, J., 1999, Water Management Techniques For Acid Mine Drainage Control: Acid Drainage Technology Initiative.

Somasundaran, P., and Agar, G. E., 1967, The zero point of charge of calcite: Journal of Colloid and Interface Science, v. 24, no. 4, p. 433-440.

Stumm, W., and Sulzberger, B., 1992, The cycling of iron in natural environments: Considerations based on laboratory studies of heterogeneous redox processes: Geochimica et Cosmochimica Acta, v. 56, no. 8, p. 3233-3257.

Sullivan, P. J., 1988, Solubility relationships of aluminum and iron minerals associated with acid mine drainage: Environmental geology and water sciences, v. 11, no. 3, p. 283-287.

Sumner, M. E., 1963, Effect of Iron Oxides on Positive and Negative Charges in Clays and Soils: Clay Minerals, v. 5, p. 218-226.

Warner, N., Acid Mine Drainage Flows through a Stream in Western Pennsylvania, National Science Foundation.

Watzlaf, G. R., Schroeder, K. T., Kleinmann, R. L., Kairies, C. L., and Nairn, R. W., 2004, The Passive Treatment of Coal Mine Drainage: United States Department of Energy National Energy Technology Laboratory Internal Publication.

Wilkin, R. T., and Barnes, H. L., 1996, Pyrite formation by reactions of iron monosulfides with dissolved inorganic and organic sulfur species: Geochimica et Cosmochimica Acta, v. 60, no. 21, p. 4167-4179.

Xu, C. Y., Schwartz, F. W., and Traina, S. J., 1997, Treatment Of Acid-Mine Water with Calcite adn Quartz Sand: Environmental Engineering Science, v. 14, no. 3.

Zhu, M., Legg, B., Zhang, H., Gilbert, B., Ren, Y., Banfield, J. F., and Waychunas, G. A., 2012, Early stage formation of iron oxyhydroxides during neutralization of simulated acid mine drainage solutions: Environ Sci Technol, v. 46, no. 15, p. 8140-8147.

Ziemkiewicz, P. F., Skousen, J. G., Brant, D. L., Sterner, P. L., and Lovett, R. J., 1997, Acid Mine Drainage Treatment With Armored Limestone In Open Limestone Channels: Journal of Environmental Quality, v. 26, no. 4, p. 1017.

APPENDIX

APPENDIX

XRD DATA

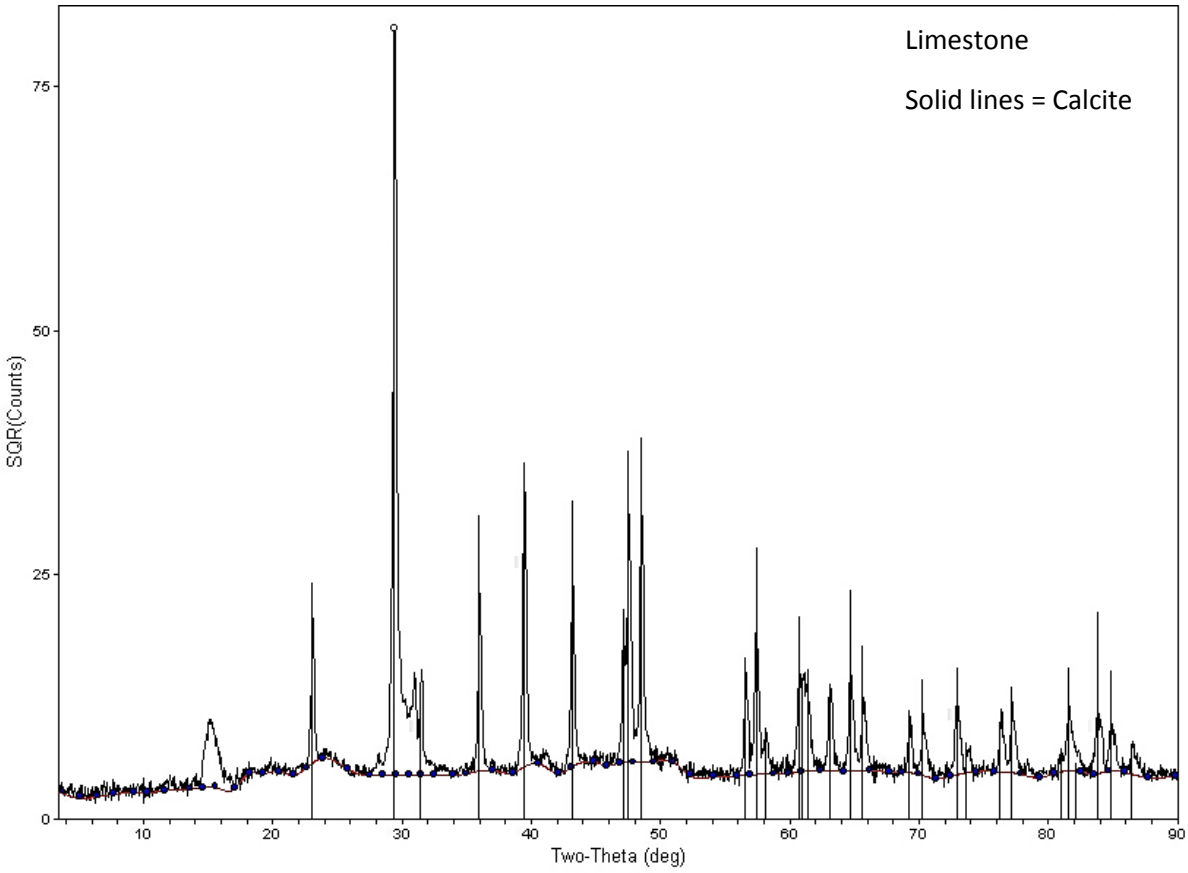

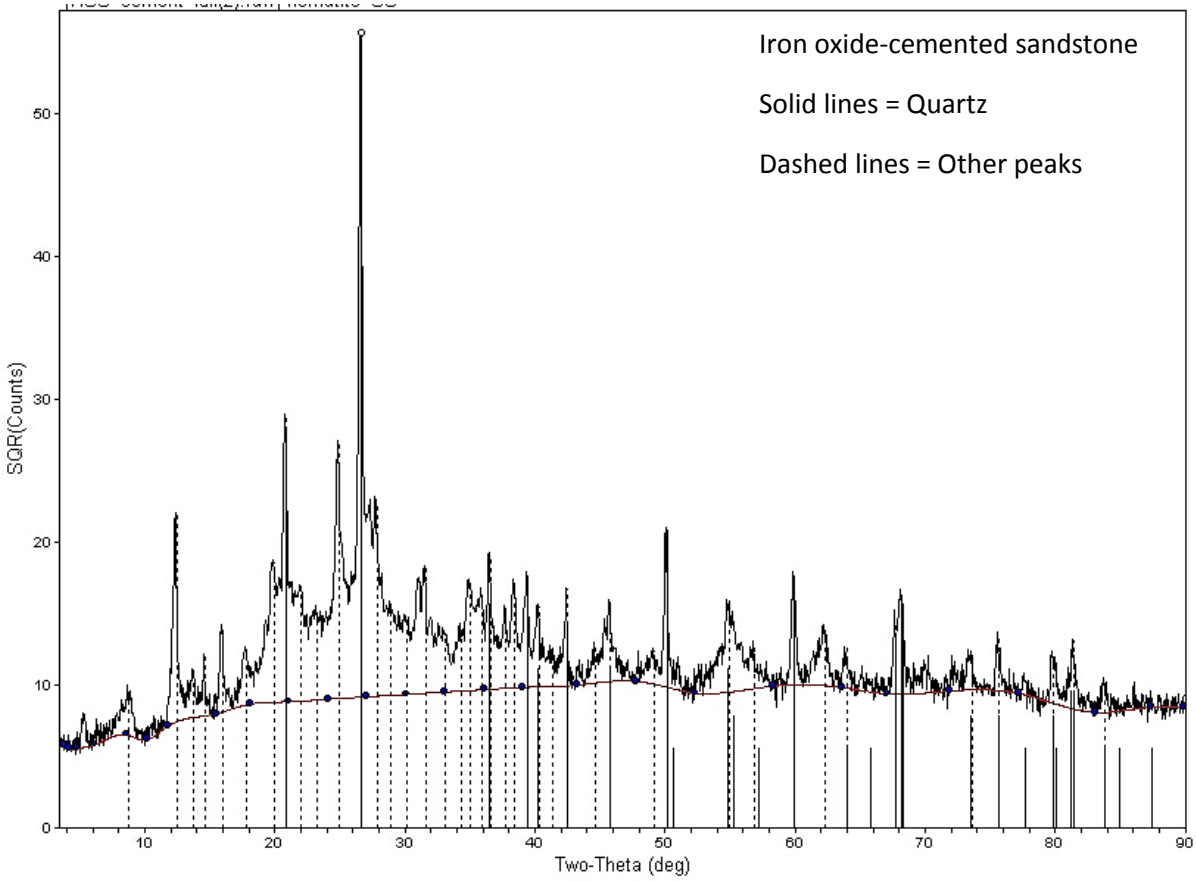
Iron oxide-cemented sandstone
Solid lines = Quartz
Dashed lines = Other peaks
SQR(Counts)
Two-Theta (deg)
0
10
20
30
40
50
60
70
80
90

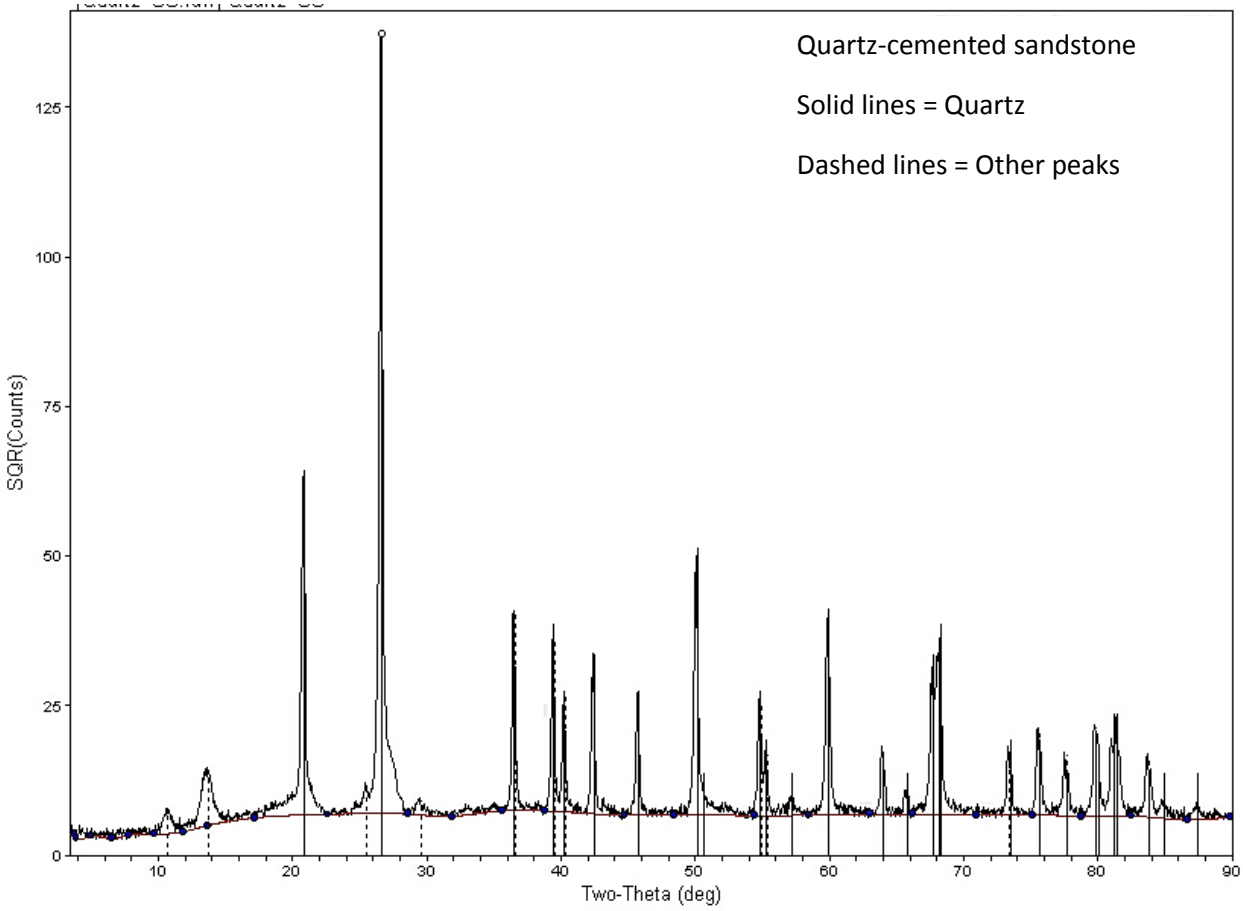
Quartz-cemented sandstone
Solid lines = Quartz
Dashed lines = Other peaks
SQR(Counts)
Two-Theta (deg)
0
25
50
75
100
125
10
20
30
40
50
60
70
80
90